

# ADVANCED FUNCTIONAL MATERIALS

## Supporting Information

for *Adv. Funct. Mater.*, DOI: 10.1002/adfm.201502340

Temperature-Dependent Charge-Carrier Dynamics in  
CH<sub>3</sub>NH<sub>3</sub>PbI<sub>3</sub> Perovskite Thin Films

*Rebecca L. Milot, Giles E. Eperon, Henry J. Snaith, Michael  
B. Johnston, and Laura M. Herz\**

## Supporting Information

### **Temperature-Dependent Charge-Carrier Dynamics in CH<sub>3</sub>NH<sub>3</sub>PbI<sub>3</sub> Perovskite Thin Films**

*Rebecca L. Milot, Giles E. Eperon, Henry J. Snaith, Michael B. Johnston, and Laura M. Herz\**

#### Contents

1. MAPbI<sub>3</sub> film characterization
2. TCSPC spectra at 8K
3. Time-resolved photoluminescence
4. Table of recombination rate constants and charge-carrier mobility
5. Fits to THz photoconductivity transients
6. Arrhenius plot for monomolecular recombination
7. Additional THz spectra
8. Charge-carrier mobility calculation
9. Plot of charge-carrier diffusion length vs. carrier density
10. References

## 1. MAPbI<sub>3</sub> film characterization

A Hitachi S-4300 field emission scanning electron microscope was used to acquire SEM images. Sample thicknesses were measured using a Veeco Dektak 150 surface profilometer. X-ray diffraction data was collected with a Panalytical X-pert Pro diffractometer.

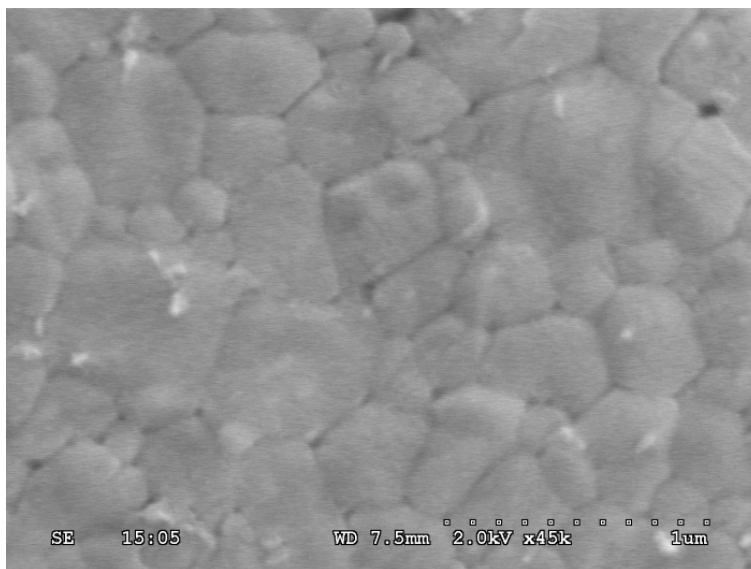


Figure S1. SEM image of the surface of a typical solvent-quenched MAPbI<sub>3</sub> film.

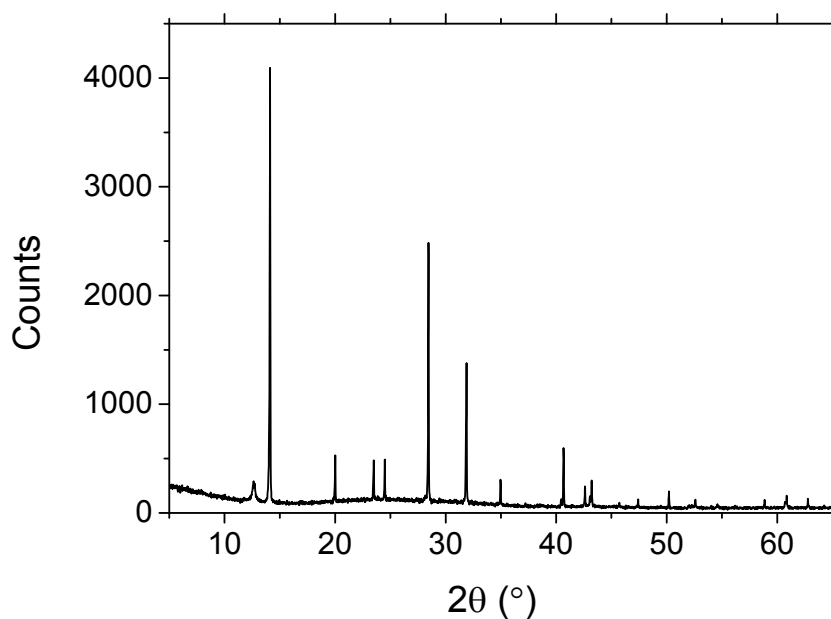


Figure S2. X-ray diffraction data for a typical solvent-quenched MAPbI<sub>3</sub> film.

## 2. Time-correlated single photon counting (TCSPC) spectra at 8K

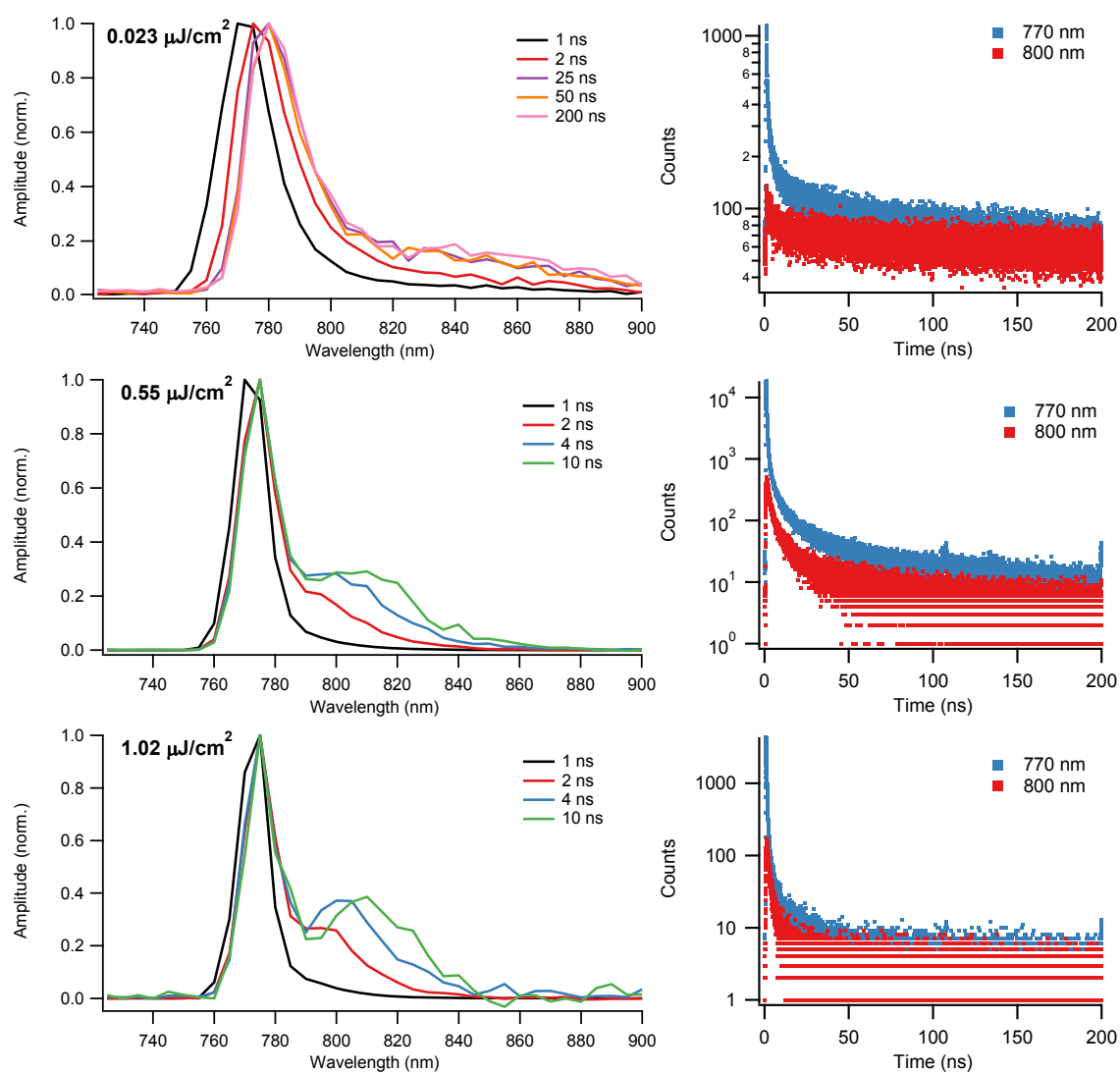


Figure S3. Left: TCSPC spectra at 8K for excitation fluences ranging from 0.023 – 1.02  $\mu\text{J}/\text{cm}^2$ . Right: PL dynamics detected at 770 and 800 nm.

### 3. Time-resolved photoluminescence

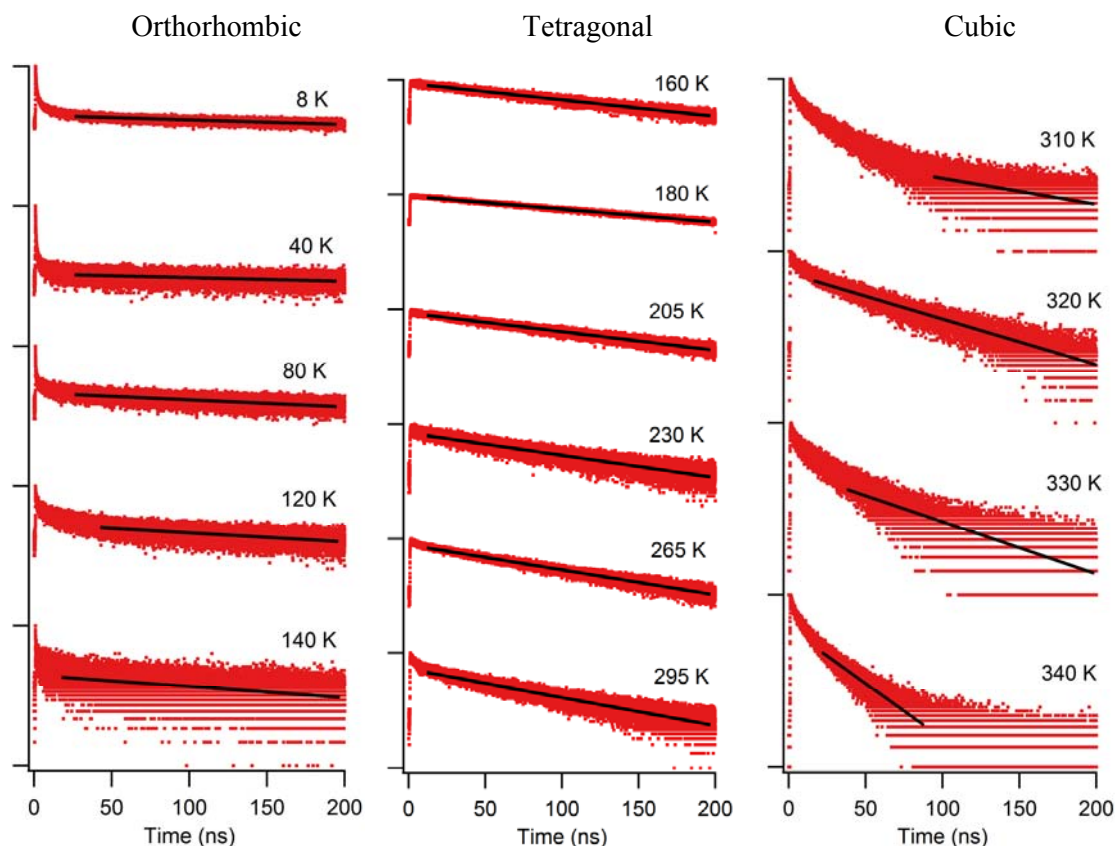


Figure S4. Time dependent PL. The sample was photoexcited at 405 nm at a fluence of 6 - 18 nJ/cm<sup>2</sup>, and PL was detected at its maximum wavelength. The red dots represent the data, and the black lines are exponential fits.

Monomolecular recombination rates  $k_f$  were extracted from the PL dynamics shown in Figure S4 through monoexponential fits to the data. For the tetragonal phase, decays were mostly fully exponential, while for the orthorhombic and cubic phases slightly faster decay components are also observed. For the orthorhombic phase, these are related to the presence of low-energy traps or inclusions<sup>[1,2]</sup> as also evident from the spectral evolution shown in Figure S3. For the cubic phase, charge-migration to traps that are predominantly located near grain boundaries and interfaces may also play a role, which can lead to deviations from exponential charge-density decay even at low fluences.<sup>[3]</sup>

## 4. Table of recombination rate constants and charge-carrier mobility

Table S1. Recombination rate constants and charge-carrier mobility.

Temp (K)	$k_1$ ( $10^6 \text{ s}^{-1}$ )	$k_2$ ( $10^{-11} \text{ cm}^3 \text{ s}^{-1}$ )	$k_3$ ( $10^{-28} \text{ cm}^6 \text{ s}^{-1}$ )	$\mu$ ( $\text{cm}^2 \text{ V}^{-1} \text{ s}^{-1}$ )
8	2.32	1650	1540	184
40	2.39	1130	2130	321
80	3.18	218	23.4	143
120	4.85	140	4.74	62
140	5.95	152	1.35	40
160	8.35	42.2	0.70	52
180	7.66	35.5	0.75	44
205	9.68	32.6	0.98	41
230	9.81	8.88	1.13	39
265	14.1	13.1	1.06	26
295	15.0	6.11	1.55	35
310	25.8	3.27	0.88	24
320	18.5	15.9	0.61	24
330	30.2	5.77	0.53	19
340	45.7	9.28	0.35	16
355	-	12.8	0.34	15
370	-	26.7	0.17	15

## 5. Fits to THz photoconductivity transients

As described in the main text, the overall recombination dynamics can be described by the following equation:

$$\frac{dn}{dt} = -k_3 n^3 - k_2 n^2 - k_1 n, \quad (\text{S1})$$

where  $n$  is the charge-carrier density,  $k_1$  is the monomolecular rate constant,  $k_2$  is the bimolecular rate constant, and  $k_3$  is the Auger rate constant.

As the experimentally observed quantity in optical pump-THz probe measurements,  $\Delta T/T = x(t)$ , is proportional to the photoconductivity, it is also proportional to the carrier density.

$$n(t) = \varphi C x(t) \quad (\text{S2})$$

The photon-to-charge branching ratio  $\varphi$  indicates the fraction of absorbed photons which are converted to charge carriers. The proportionality factor  $C = \tilde{n}_0/x(0)$  is the ratio of the absorbed photon density  $\tilde{n}_0$  to the initial THz response at time zero  $x(0)$ , where

$$\tilde{n}_0 = \frac{E\lambda\alpha(\lambda)}{hcA_{\text{eff}}}(1 - R_{\text{pump}}). \quad (\text{S3})$$

The absorbed photon density is a function of the absorption coefficient  $\alpha$  and reflectance  $R_{\text{pump}}$  of the sample at the excitation wavelength  $\lambda$  and of the effective overlap  $A_{\text{eff}}$  of the optical pump beam and THz probe beam. At high excitation fluences,  $x(0)$  is no longer proportional to  $\tilde{n}_0$ . The value of  $C$  is therefore determined using a value of  $x(0)$  within the regime where  $x(0)$  is linearly proportional to the excitation fluence.

An expression for the time-dependent THz dynamics can be obtained by substituting Equation S2 into Equation S1:

$$\begin{aligned} \frac{dx}{dt} &= -C^2\varphi^2 k_3 x^3 - C\varphi k_2 x^2 - k_1 x \\ &= -A_3 x^3 - A_2 x^2 - A_1 x \end{aligned} \quad (\text{S4})$$

with  $A_i = C^{i-1}\varphi^{i-1}k_i$ . The coefficients  $A_1$ ,  $A_2$ , and  $A_3$  are determined via a global fit to a fluence dependent set of THz transients. As the photon-to-free-carrier conversion ratio  $\varphi$  is unknown, we can only determine the values  $\varphi^2 k_3$ ,  $\varphi k_2$  and  $k_1$  from our fits. These equal the actual decay rate constants  $k_3$ ,  $k_2$  and  $k_1$  in case the material exhibits full photon-to-free-charge conversion and are lower limits when  $\varphi < 1$ .

To account for the spatially varying charge density profile, the fit routine takes into account the exponential charge density profile created by the pump beam by dividing the sample into 50 equally thick slabs and computing the decay function for all of these individually.

## 6. Arrhenius plot for monomolecular recombination

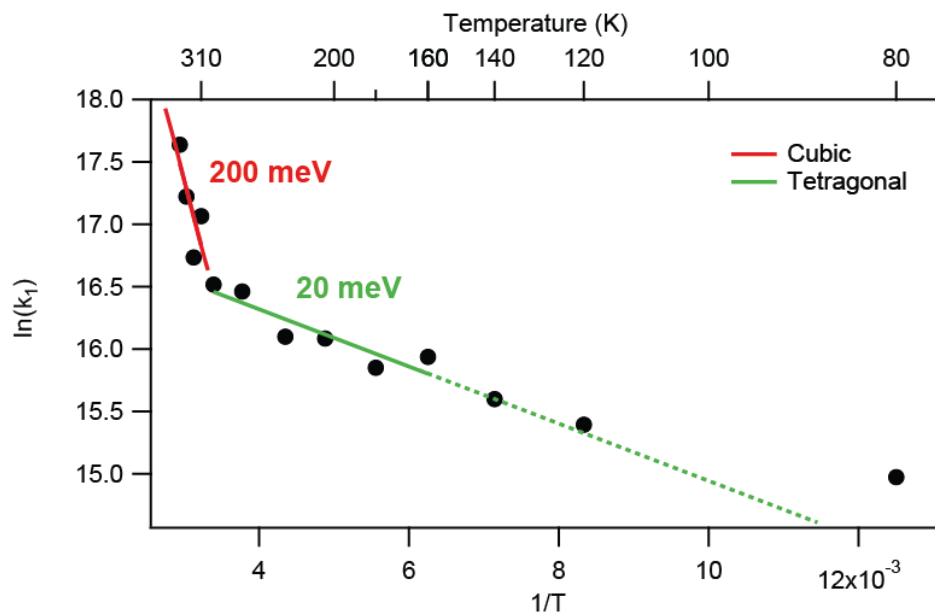
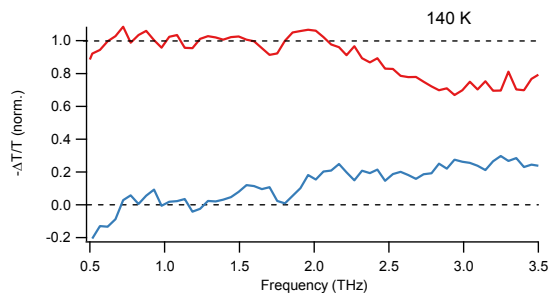
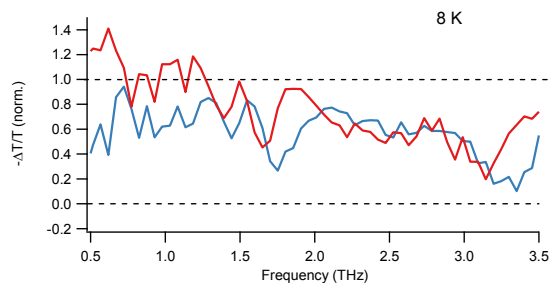


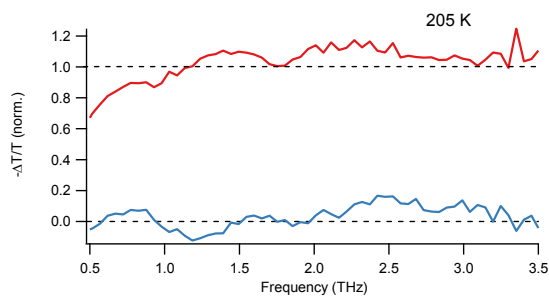
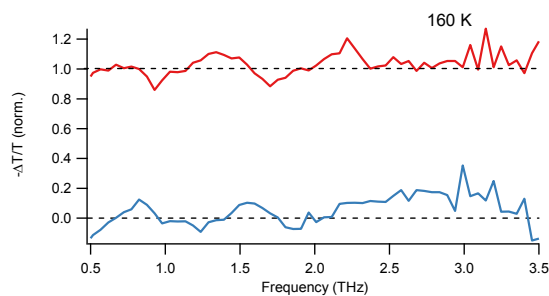
Figure S5. Arrhenius plot for the monomolecular rate constant. Activation energies of  $200 \pm 100$  meV and  $20 \pm 5$  meV were calculated for the cubic and tetragonal phases, respectively. An extension of the trend for the tetragonal phase into the orthorhombic phase (green, dashed line) suggests that the activation energy is similar at temperatures near the phase transition temperature. Deviations from linearity at low temperature may arise from excitonic recombination, which increases the monomolecular decay rate that is dominated by free-charge trapping at higher temperatures.

## 7. Additional THz spectra

### Orthorhombic



### Tetragonal



### Cubic

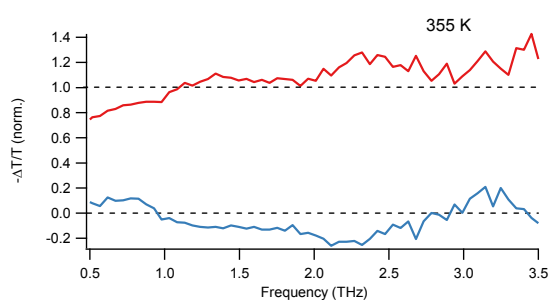
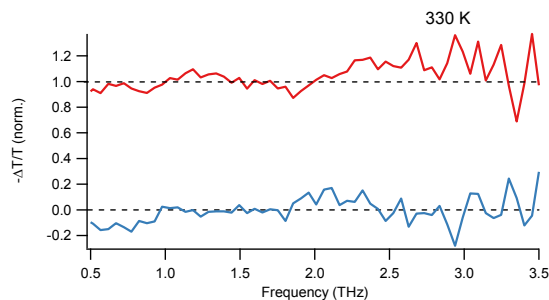


Figure S6. THz spectra at additional temperatures in each phase. For all spectra, the delay time between the 550-nm optical pump pulse and THz probe pulse was 5 ps. The imaginary parts of the conductivity are shown in blue, and the real parts are shown in red.

## 8. Charge-carrier mobility calculation

The charge carrier mobility  $\mu$  is given by

$$\mu = \frac{\Delta S A_{\text{eff}}}{Ne}, \quad (\text{S5})$$

where  $\Delta S$  is the sheet conductivity of the perovskite thin film,  $A_{\text{eff}}$  is the effective area of the overlap of optical pump and THz probe pulse,  $N$  is the number of photoexcited charge carriers, and  $e$  is the elementary charge.

Assuming that the film thickness is much smaller than the THz wavelength, the sheet photoconductivity  $\Delta S$  of a thin film between two media of refractive indices,  $n_A$  and  $n_B$ , can be expressed as<sup>[4, 5]</sup>

$$\Delta S = -\varepsilon_0 c (n_A + n_B) \left( \frac{\Delta T}{T} \right), \quad (\text{S6})$$

where  $\Delta T/T$  is the experimentally determined change in transmitted THz electric field amplitude. In our experiment,  $n_A = 1$  for vacuum and  $n_B = 2.13$  for the z-cut quartz substrate.

The number of photo-excited charge carriers  $N$  can be determined using the following equation:

$$N = \varphi \frac{E\lambda}{hc} (1 - R_{\text{pump}}) (1 - T_{\text{pump}}), \quad (\text{S7})$$

where  $E$  is the energy contained in an optical excitation pulse of wavelength  $\lambda$ ,  $R_{\text{pump}}$  is the reflectivity of the sample at normal incidence of the excitation beam,  $T_{\text{pump}}$  transmittance of the pump beam, and  $\varphi$  is the ratio of free charge carriers created per photons absorbed (the photon-to-charge branching ratio). Although  $\varphi$  is undetermined, its value can be assumed to be unity if the conductivity is Drude-like, which is valid for most of the temperatures examined here.

Substituting Equations S7 and S6 into Equation S5, the following equation is obtained:

$$\varphi\mu = -\varepsilon_0 c (n_A + n_B) \frac{A_{\text{eff}} hc}{Ee\lambda (1 - R_{\text{pump}}) (1 - T_{\text{pump}})} \left( \frac{\Delta T}{T} \right). \quad (\text{S8})$$

Because  $0 \leq \varphi \leq 1$ , the effective mobility  $\varphi\mu$  represents a lower limit, which becomes identical to the actual mobility for full photon to free carrier conversion. To allow accurate determination of  $\varphi\mu$ , we ensured that excitation conditions were in the linear regime. It should also be noted that the determined charge carrier mobility arises from the contributions of both electrons and holes and that these contributions cannot be separated.

## 9. Plot of charge-carrier diffusion length vs. carrier density

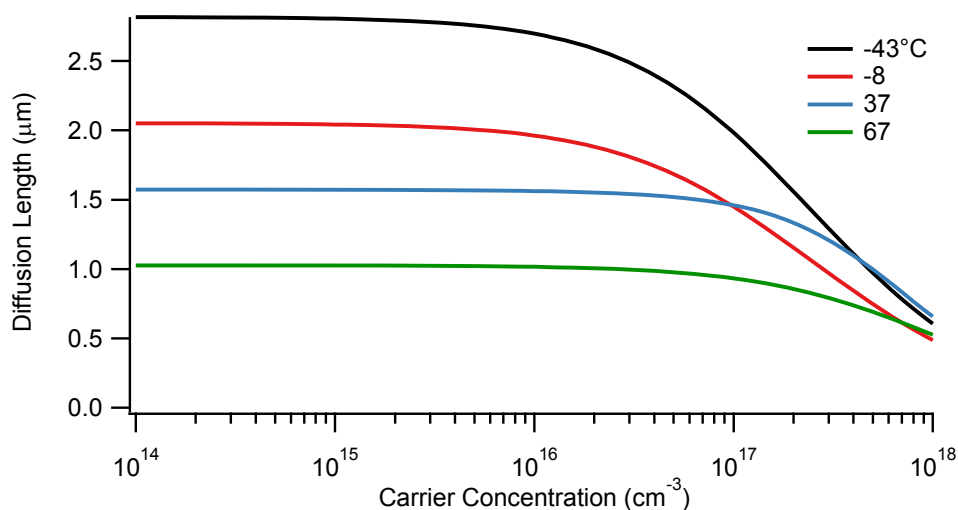


Figure S7. The diffusion length as a function carrier concentration for temperatures relevant to device performance. Although the diffusion length is decreased at higher temperatures, the decreases in  $k_2$  and  $k_3$  in the cubic phase ensure that this value is maintained for much higher fluences. The diffusion length at temperatures in the tetragonal phase ( $-43^\circ\text{C}$  and  $-8^\circ\text{C}$ ) begins to decrease near a charge-carrier density of  $10^{16}\text{ cm}^{-3}$  and is decreased by about 75% by  $10^{18}\text{ cm}^{-3}$ . In contrast, the diffusion length at temperatures in the cubic phase ( $37^\circ\text{C}$  and  $67^\circ\text{C}$ ) does not start to decrease until  $10^{17}\text{ cm}^{-3}$  and only decreases by about 30% by  $10^{18}\text{ cm}^{-3}$ . Although these carrier densities are outside the operating range for standard cells, they are applicable to concentrator systems, where the excitation intensity can exceed 150 suns.

## 10. References

- [1] C. Wehrenfennig, M. Z. Liu, H. J. Snaith, M. B. Johnston, L. M. Herz, *APL Mater.* **2014**, 2, 081513.
- [2] X. X. Wu, M. T. Trinh, D. Niesner, H. M. Zhu, Z. Norman, J. S. Owen, O. Yaffe, B. J. Kudisch, X. Y. Zhu, *J. Am. Chem. Soc.* **2015**, 137, 2089.
- [3] D. W. deQuilettes, S. M. Vorpahl, S. D. Stranks, H. Nagaoka, G. E. Eperon, M. E. Ziffer, H. J. Snaith, D. S. Ginger, *Science* **2015**, 348, 683.
- [4] R. Ulbricht, E. Hendry, J. Shan, T. F. Heinz, M. Bonn, *Rev Mod Phys* **2011**, 83, 543.
- [5] H. K. Nienhuys, V. Sundström, *Phys. Rev. B* **2005**, 71.